Navigating phase boundaries: analyzing phase change paths of water within canisters in phase diagrams during vacuum drying

Ji Hwan Lim [a,*], Kyoung-Sik Bang [a], Kyung-Wook Shin [b], Nam-Hee Lee [b], Seung-Hwan Yu [a]

[a] *Transportation and Storage R&D Section, Korea Atomic Energy Research Institute, 111 Daedeok-daero 989 beon-gil, Yuseong-gu, Daejeon 34057, Republic of Korea*
[b] *SAE-AN Eng, Corp.,481-10 Gasan-dong Geumcheon-gu, Seoul 08501, Republic of Korea*
[*] *Corresponding author: jlim@kaeri.re.kr*
***Keywords :** Vacuum drying, Spent nuclear fuel, Dry storage system, Residual water, Heat-transfer

1. Introduction

The wet storage facilities at domestic nuclear power plants have begun to approach saturation [1]. The storage capacities of Kori, Hanbit, and Hanul nuclear power plants are nearing their limits at 83.8%, 74.2%, and 80.8% respectively [2]. The use of dry storage for spent nuclear fuel (SNF) is anticipated to address the spatial limitations of the current wet storage within nuclear reactors. Dry storage involves placing SNF in containers made of concrete or metal, designed to withstand continuous radiation and high heat emissions. Not only at the Wolsong nuclear power plant in Korea but also in 17 out of 31 nuclear-operating countries worldwide, dry storage has demonstrated technical excellence and safe management of SNF [3]. It has the advantage of using passive natural cooling, which does not require an external power supply, and poses no risk of radiation leakage even in unexpected natural disasters like earthquakes. Moreover, the multi-layer shielding in dry storage facilities ensures low radiation levels, averaging between 0.009-0.018 mSv (with the permissible dose for the public being 1 mSv), reflecting high safety standards [3].

However, residual moisture in SNF can cause degradation of internal structures and the fuel itself, making complete water removal from the container crucial before entering the vacuum drying stage. Given that Korea is preparing to adopt dry storage while also needing to predict and address potential long-term safety issues like creep, hydride reorientation, and degradation, technical data on the dried state of SNF post-vacuum drying is indispensable. Currently, the direct measurement of cladding temperature or drying levels inside containers under the approved conditions (sustaining 3 torr for 30 minutes) post-vacuum drying remains challenging. Consequently, it is necessary to identify and quantify factors influencing residual water through vacuum drying tests. Even meeting the drying criteria, industrial and academic evaluations suggest that considerable residual water could remain, underscoring the importance of this experiment [4]. In the United States, it has been recognized that residual hydrogen can lead to hydride formation within the SNF cladding, posing a significant risk to maintaining the integrity of fuel rods during potential future retrievals. This awareness has spurred numerous studies [5]. Researchers from the University of South Carolina noted that quantifying residual water using indirect indicators like pressure increases is often inaccurate, thus emphasizing the importance of theoretical models. Theoretical models can predict detailed data such as temperature, evaporated water quantity, and ice formation, using a theoretical approach applicable under a wide range of conditions. However, as mentioned in their paper, these models cannot resolve multi-physical phenomena and are not suitable for complex geometries like the assemblies comprising several fuel rods, spacer grids, plates, piping, springs, and cladding within actual SNF [5]. Internal structures such as basket frameworks, cask bottoms, and spacer grids provide flat surfaces where substantial water can accumulate, complicating multi-dimensional modeling efforts during the vacuum drying stage.

Hence, before developing theoretical vacuum drying heat transfer and residual water prediction models, some studies have explored simulation methods using computational resources [6-8]. In 1996, Kawasaki Heavy Industries used the Zephyrus code to develop an initial simulation model, implementing a 2D section of a horizontally arranged dry storage canister scaled down by five times, and simulating natural convection under low flow conditions [6]. Later, researchers from Tsinghua University in China improved upon this by incorporating forced convection heat transfer effects into the simulations [7]. However, both studies were limited to predicting heat transfer performance during vacuum drying and did not extend to residual water prediction. Researchers at the University of Nevada, led by Greiner, addressed the challenge of simulating SNF with multi-rod assemblies and complex geometries using 2D computational fluid dynamics (CFD) frameworks, ignoring convection effects to focus on accurately predicting heat transfer and temperatures within the fuel rods [8]. Their work was significant in paving the way for 3D heat transfer simulations using CFD tools, with subsequent studies offering meaningful results by predicting axial temperatures using concentrated computational models [9-10]. Nevertheless, they demonstrated that rapid pressure reduction conditions induced boiling and ice formation, complex phenomena essential for predictive accuracy but difficult to simulate, thus reinforcing the necessity

of experimental validation for residual water prediction in vacuum drying [9-10].

Despite these efforts, additional research is crucial to identify significant thermodynamic factors influencing residual water during the vacuum drying process, particularly considering pump capacity and volume, given that many prior studies were based on simplifications. In this study, the research team conducted a thermodynamic evaluation aimed at enhancing evaporation efficiency compared to traditional step-wise pressure reduction methods and performed residual water quantification based on drying requirements (3 torr for 30 minutes). The detailed experimental results are discussed in the following sections.

2. Experimental methods and procedures

The lab-scale vacuum drying test apparatus used for the experiments consists of a canister, an operation control panel, a cold trap, and a rotary vane pump. The apparatus is equipped with a measurement system designed to record various parameters, such as temperature, pressure, weight, and moisture, in order to evaluate the amount of residual water drying out within the canister during the test. The canister, integral to the lab-scale vacuum drying apparatus, is fabricated from acrylic material to allow visual observation of the water state changes during the drying process. To assess the impact of canister volume on the drying efficiency, two canisters with diameters of 50 cm and heights of 50 cm and 100 cm were constructed, as illustrated in Figure 1 [11-12]. The operation control panel regulates the function of the equipment within the lab-scale vacuum drying setup. This control panel comprises multiple components, including the main power switch, rotary vane pump, root pump, cold trap 1, cold trap 2, panel fan, and control power.

Fig. 1. Lab-scale vacuum drying test setup overview.

To capture vaporized water during the vacuum drying process and prevent it from entering the vacuum pump, a cold trap is employed. The cold trap used in this experiment is the CT-4.8G model from “LabHouse,” which has a bath volume capacity of 4.8 liters. Rotary vane pumps of different capacities (200, 400, and 600 l/min) from "Wosung Vacuum Pump" (models MVP 12, MVP 24, and MVP 36) were selected to evaluate the effect of pump capacity on the drying efficiency, with images of these pumps shown in Figure 2. The measurement system for the lab-scale vacuum drying test includes several modules from National Instruments (NI), namely the NI-9214, NI-9253, cDAQ-9174, and the Multi-4U COMBO unit. The NI-9214 module is used to detect analog signals from thermocouples installed in the canister and water to measure temperature, supporting up to 16 thermocouples. The NI-9253 module detects analog signals from sensors measuring flow and dew point temperature, also supporting up to 16 sensors. The cDAQ-9174 chassis connects up to four modules, including those for thermocouples and dew point sensors, and converts these analog signals to digital form. The Multi-4U COMBO unit, comprised of four channels, converts analog signals from micro-balances and pressure sensors to digital data. All signals are subsequently analyzed and stored by a LabView Software-based residual water measurement program installed on the computer, allowing for real-time monitoring of temperature changes during the test.

Fig. 2. Various capacity pumps used in the experiment.

The experimental procedure follows the guidance from NRC-02-07-C-006 [13], which recommends a slow or stepwise reduction of pressure to prevent ice formation by allowing the system time to reach equilibrium. However, using a pump with too low capacity can extend the drying time. Therefore, selecting an appropriate pump capacity is crucial. The vacuum drying tests were conducted by using vacuum pumps with capacities of 200, 400, and 600 l/min to evaluate their impact on the drying process. The procedure includes connecting the selected vacuum pump to the apparatus, powering on the lab-scale vacuum drying setup, and waiting until the cold trap temperature falls below -20 °C. Water is then filled to the test volume in a beaker, and the canister lid is

opened to place the beaker on the micro-balance inside the canister. After adjusting the thermocouples, the lid is closed and secured. The computer and measurement instruments are activated, and the appropriate software is run to start the measurement process. The vacuum pump operates until the water surface temperature reaches approximately 0.1 °C, after which the program is stopped, and the apparatus is powered down. Finally, the canister is brought back to atmospheric pressure, and the beaker is removed and cleaned of any residual water. The measurement systems utilized include two types for monitoring four key parameters: temperature (water temperature), pressure (internal canister pressure), weight (water weight), and moisture (dew point temperature).

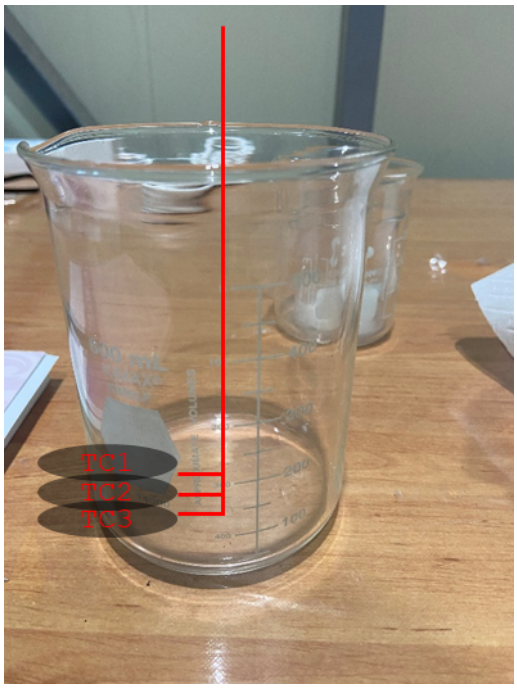

Fig. 3. Beaker for water containment and placement of Thermocouples (TC) with intervals.

The initial experimental conditions are detailed as follows:

- Canister heights of 0.5m and 1m
- Beaker capacity of 600 mL
- Thermocouple intervals of 4.5 mm (Figure. 3)
- Initial water height of 1.8 cm
- Beaker inner diameter of 88 mm
- Vacuum pump capacities of 100, 200, 400, and 600 L/min
- Initial water conditions of 40°C and 100g
- An evaporation area of 6082.12 mm²
- Presence or absence of vacuum stages and stage holding time
- Physical properties based on NIST data

The vacuum drying tests were performed with an initial water temperature of 40°C, similar to the water temperature in spent nuclear fuel storage pools (around 40°C to 45°C), to simulate realistic conditions for the residual water in the canister. In this section some of the techniques used to model the detector channel are described. The channel model includes a SiC detector, cable, preamplifier, amplifier, and discriminator models.

3. Result and discussion

3.1 Direct Depressurization

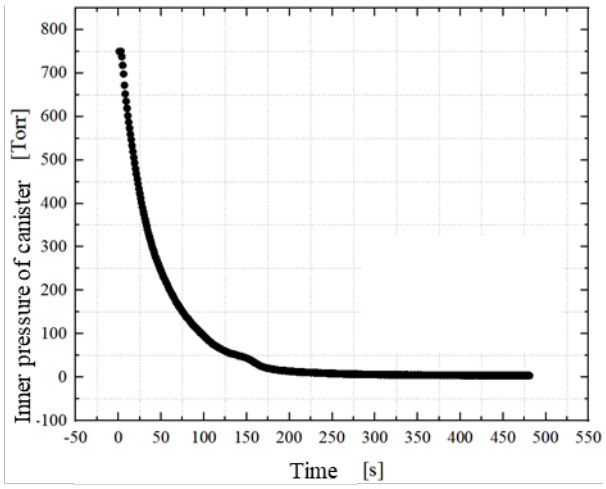

Fig. 4. Pressure Variation Inside the Canister Over Time (Pump Capacity: 400 L/min, Initial Water Condition: 40°C, Canister Height: 0.5 m).

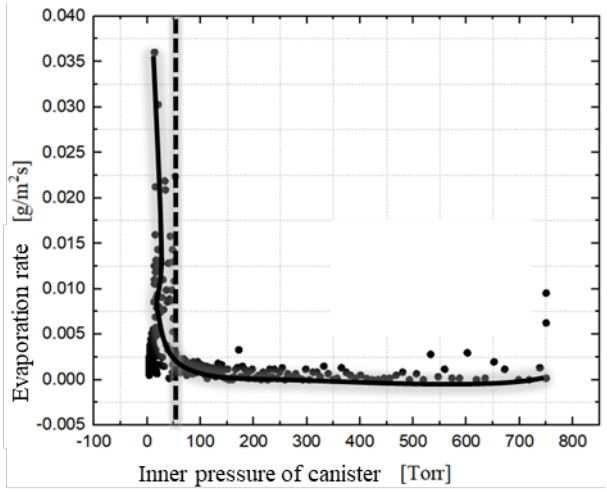

Fig. 5. Evaporation Rate Variation Over Time (Pump Capacity: 400 L/min, Initial Water Condition: 40°C, Canister Height: 0.5 m).

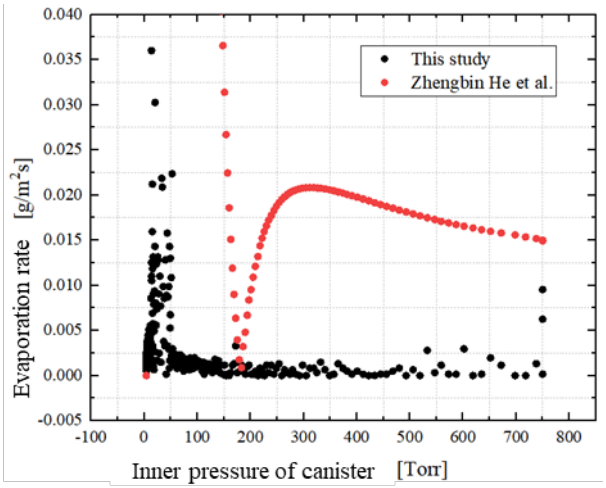

Fig. 6. Comparison of Evaporation Rate Variation with Previous Correlation Values (Pump Capacity: 400 L/min, Initial Water Condition: 40°C, Canister Height: 0.5 m).

In Figure 4, the trend of directly reducing the internal canister pressure to below 3 torr over time, using a pump with a capacity of 400 L/min, initial water condition of 40°C, and canister height of 0.5 m, is illustrated. By tracking the precise residual water mass measured using a precision balance and converting it to evaporation rate, we can produce a graph as shown in Figure 5. During the pressure reduction, the water does not evaporate at a constant rate. Instead, the rate significantly increases below approximately 50 torr, following an L-shaped curve. Upon checking whether this trend is reflected in the correlation derived from previous studies on evaporation rates during vacuum drying, as seen in Figure 6, the Z.B. He correlation [14] also shows a sharp increase in evaporation rate beyond a certain pressure point. This critical pressure point was identified as the boundary line between the liquid and gaseous phases on the water phase equilibrium diagram. The discrepancy between the critical points in the correlation and the experimental data can be attributed to the nature of Z.B. He's correlation, which assumes the vacuum drying of wood rather than the conditions of this study. The results of converting the evaporation rate and latent heat during the vacuum drying process into surface heat transfer coefficients are presented in Figure 7. This graph shows that the heat transfer coefficient varies with internal canister pressure yet remains similar to the values predicted by Z.B. He's correlation. Figure 8 evaluates the heat transfer rate within the water using thermocouples placed at varying intervals within the beaker. The results show that the upper portion of the residual water cools more rapidly, with the cooling rate increasing as the pressure is further reduced.

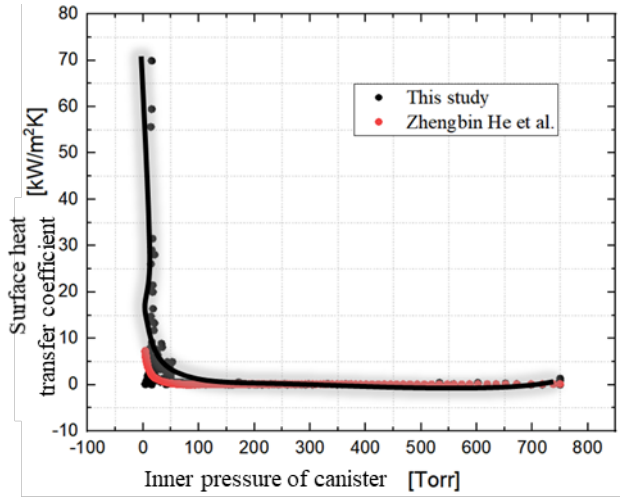

Fig. 7. Comparison of Surface Heat Transfer Coefficient Variation with Previous Correlation Values (Pump Capacity: 400 L/min, Initial Water Condition: 40°C, Canister Height: 0.5 m).

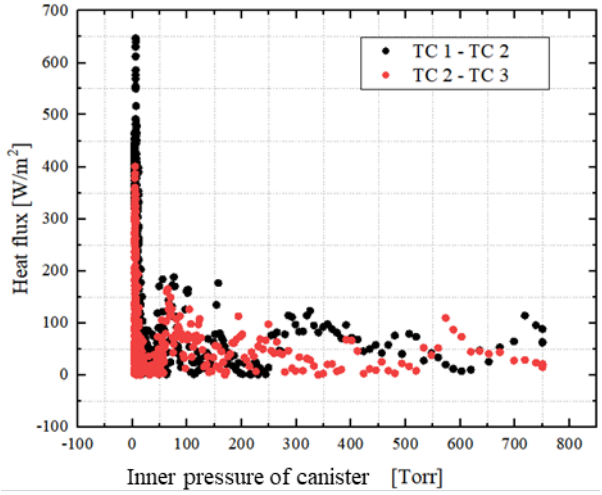

Fig. 8. Heat Flux Variation Inside Water as a Function of Canister Pressure Variation (Pump Capacity: 400 L/min, Initial Water Condition: 40°C, Canister Height: 0.5 m).

3.2 Stepwise Depressurization (Conventional Method)

While the previous section analyzed the direct depressurization method, commercial vacuum drying stages typically employ stepwise pressure reduction to avoid safety issues such as ice formation and rapid temperature changes. Figure 9 illustrates the stepwise reduction in internal pressure over time during the stepwise depressurization. Figure 10 graphs the evaporation rate under stepwise depressurization, showing a temporary increase in evaporation during the hold time as the internal moisture diffuses and fills the canister. Figure 11 confirms a quicker entry into the "evaporation promotion zone" with hold time compared to transient conditions. However, the extent of this effect is minimal, suggesting that the evaporation promotion zone's impact is delayed in transient conditions compared to thermal equilibrium. In Figure 12, the heat flux change inside the water varies with the

hold time, showing a pattern of rising and falling corresponding to each hold stage.

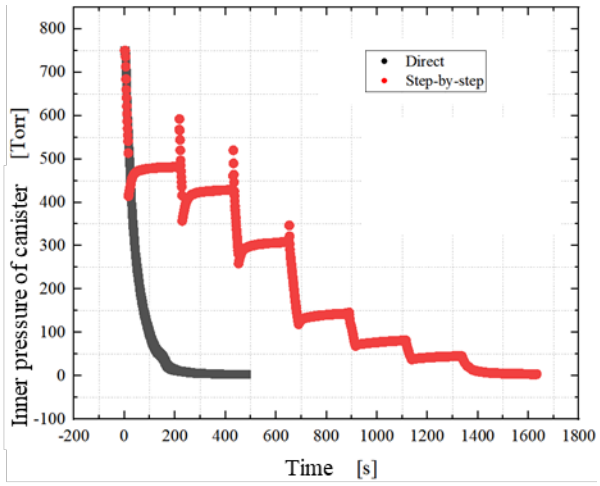

Fig. 9. Pressure Variation Inside the Canister Over Time During Step-Wise Depressurization (Pump Capacity: 400 L/min, Initial Water Condition: 40°C, Canister Height: 0.5 m).

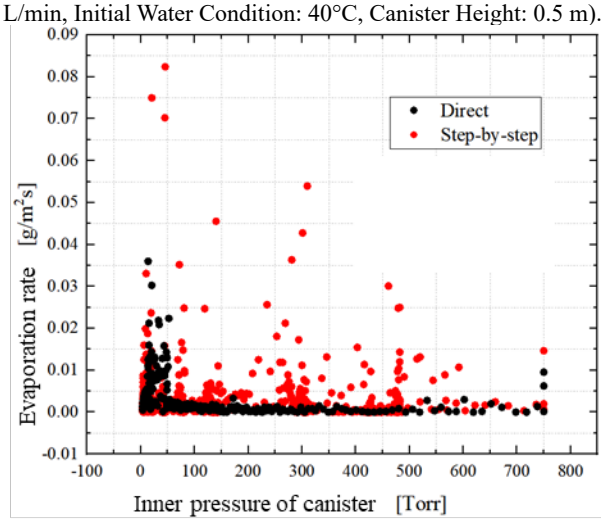

Fig. 10. Evaporation Rate Variation Over Time During Step-Wise Depressurization (Pump Capacity: 400 L/min, Initial Water Condition: 40°C, Canister Height: 0.5 m).

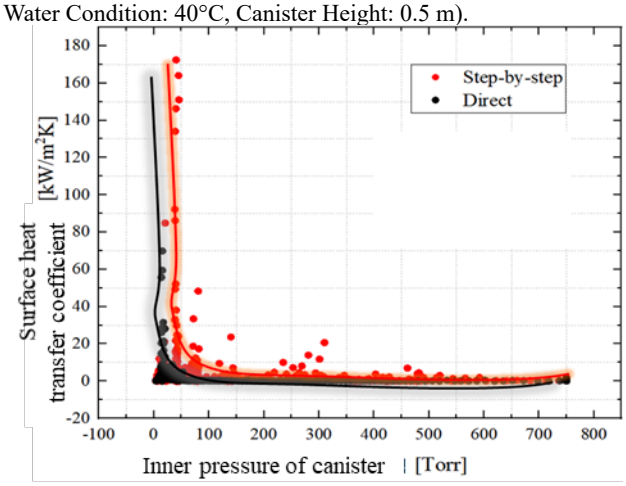

Fig. 11. Variation of Surface Heat Transfer Coefficient as a Function of Canister Pressure (Pump Capacity: 400 L/min, Initial Water Condition: 40°C, Canister Height: 0.5 m).

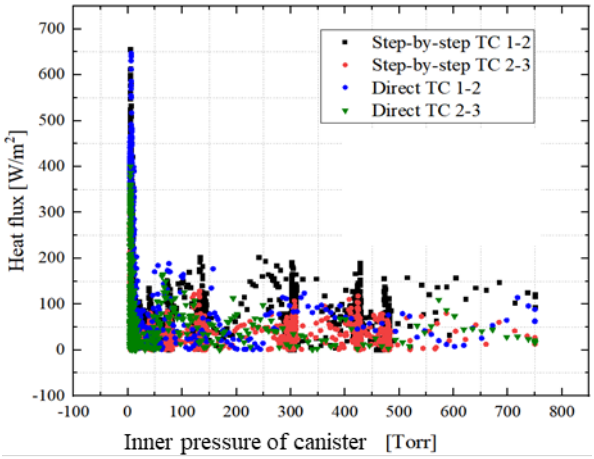

Fig. 12. Heat Flux Variation Inside Water During Step-Wise Depressurization as a Function of Canister Pressure (Pump Capacity: 400 L/min, Initial Water Condition: 40°C, Canister Height: 0.5 m).

3.3 Activation of Evaporation Promotion Zone

To enhance the evaporation promotion zone and effectively evaporate residual water in a shorter time, the research team compared three vacuum drying methods. These are: (1) the current stepwise decompression method to prevent ice formation, (2) a stepwise decompression method after entering the phase equilibrium boundary (hold: 25 minutes), and (3) repeating the hold and re-entry after reaching the phase equilibrium boundary (hold: 5 minutes). The pressure variation process and the change in water surface temperature for these methods are shown in Figures 13 and 14, respectively. The evaporation efficiency comparison results are presented in Table I. Strategy 2 showed the highest improvement in evaporation efficiency, recording a 92% increase, nearly double the efficiency of the conventional method. Strategy 3 showed a lesser improvement of 62%, presumed due to a decrease in efficiency upon re-entering the evaporation promotion zone compared to the initial entry.

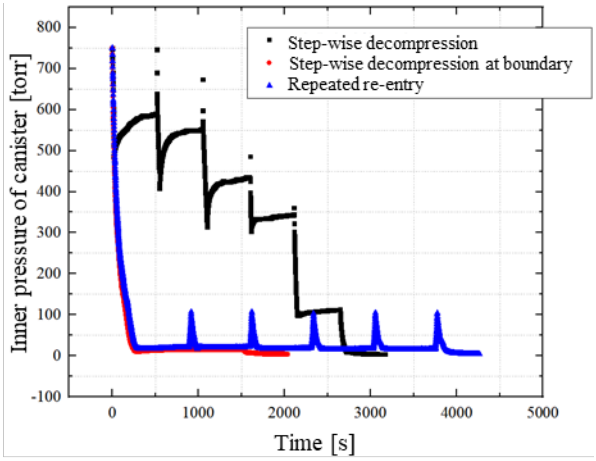

Fig. 13. Pressure Variation Inside the Canister Over Time (Three Different Vacuum Drying Strategies).

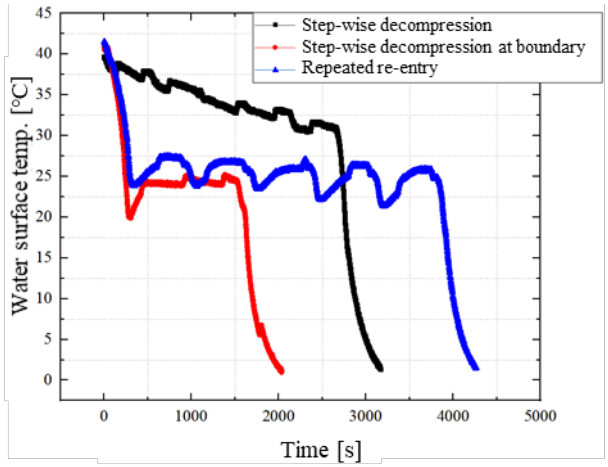

Fig. 14. Variation of Water Surface Temperature Over Time (Three Different Vacuum Drying Strategies).

Table I: Summary of Evaporation Efficiency for Three Different Vacuum Drying Strategies

	Initial hold pressure	**Hold time[min]**	**Efficiency [mg/s]**	**Evaporation efficiency**
Step-wise decompression (conventional method)	400 torr	10	9.668	1.0
Step-wise decompression at phase change boundary	phase change boundary	25	18.526	1.92
Repeated re-entry after entering phase change boundary	phase change boundary	5	15.709	1.62

4. Conclusions

This study quantitatively evaluated the evaporation rate of residual water inside the canister in relation to changes in pressure over time using lab-scale vacuum drying test equipment. Experimental findings reported a significant increase in evaporation rate beyond a specific pressure range during the depressurization stage. Additionally, comparisons between direct and stepwise depressurization methods demonstrated differences in heat transfer within residual water, evaporation rate, and efficiency. Lastly, this study assessed strategies to maximize evaporation efficiency by holding at the evaporation promotion zone, yielding up to a 92% improvement over conventional methods. Future studies aim to extend these findings beyond lab-scale to pilot-scale evaluations and develop commercially viable vacuum drying methods with enhanced thermodynamic evaporation efficiency.

Acknowledgements

This work was supported by the Institute for Korea Spent Nuclear Fuel (iKSNF) and National Research Foundation of Korea (NRF) grant funded by the Korea government (Ministry of Science and ICT, MSIT) (No. 2021M2E1A1085226).

REFERENCES

[1] S. Choi, J. Lim, “A Review on Sabotage against Transportation of Spent Nuclear Fuel.” *Trans. Korean Nuclear Society Autumn Meeting* (2016).
[2] "KHNP Nuclear Power Plants," Korea Hydro & Nuclear Power. [Online]. Available: https://npp.khnp.co.kr/index.khnp?menuCd=DOM_000000103004004001
[3] "Spent nuclear fuel undergoes testing," Dnews, 8-May-2022. [Online]. Available: https://m.dnews.co.kr/m_home/view.jsp?idxno=202205080808564610942
[4] Bang, K. S., Yu, S. H., & Shin, K. W. (2021). Experimental investigation of vacuum drying for removal of residual water in canister. Annals of Nuclear Energy, 156, 108185.
[5] Saha, S., Khan, J., Knight, T., & Farouk, T. (2022). A global model for predicting vacuum drying of used nuclear fuel assemblies. Nuclear Technology, 208(3), 414-427.
[6] Nishimura, M., Shibazaki, H., Fujii, S., & Maekawa, I. (1996). Natural convection heat transfer in the horizontal dry storage system for the LWR spent fuel assemblies. Journal of nuclear science and technology, 33(11), 821-828.
[7] Heng, X., Zuying, G., & Zhiwei, Z. (2002). A numerical investigation of natural convection heat transfer in horizontal spent-fuel storage cask. Nuclear Engineering and Design, 213(1), 59-65.
[8] Araya, P. E., & Greiner, M. (2007, January). Use of regular rod arrays to model heat transfer from BWR fuel assemblies inside transport casks. In ASME Pressure Vessels and Piping Conference (Vol. 42851, pp. 521-528).
[9] Li, J., & Liu, Y. Y. (2016). Thermal modeling of a vertical dry storage cask for used nuclear fuel. Nuclear Engineering and Design, 301, 74-88.
[10] Tseng, Y. S., Wang, J. R., Tsai, F. P., Cheng, Y. H., & Shih, C. (2011). Thermal design investigation of a new tube-type dry-storage system through CFD simulations. Annals of Nuclear Energy, 38(5), 1088-1097.
[11] Bang, K. S., Lim, J. H., Yu, S. H., Shin, K. W., Lee, N. H., & Chae, G. S. (2023). Drying Tests According to Pump Capacity and Canister Volume. Korean Radioactive Waste Society Conference Paper, 21(2), 146-146.
[12] Lim, J. H., Bang, K. S., Shin, K. W., Lee, N. H., & Yu, S. H. (2023). Experimental-Parametric Study on Residual Water During Vacuum Drying of Spent Nuclear Fuel Canisters. Korean Radioactive Waste Society Conference Paper, 21(2), 145-145.
[13] NRC-02-07-C-006, “Vacuum Drying Test Plan-Public Version“, U.S. NRC Washington, DC, July 2013.
[14] He, Z. B., Zhao, Z. J., Zhang, Y., Lv, H., & Yi, S. L. (2015). Convective heat and mass transfer during vacuum drying process. Wood Res, 60, 929-38.